NASA TECHNICAL MEMORANDUM

NASA TM X-71595

NASA TM X-71595

EXPERIMENTAL AND ANALYTICAL SONIC NOZZLE DISCHARGE COEFFICIENTS FOR REYNOLDS NUMBERS UP TO 8×10^6

by Andrew J. Szaniszlo
Lewis Research Center
Cleveland, Ohio 44135

TECHNICAL PAPER proposed for presentation at
Winter Annual Meeting of the American Society
of Mechanical Engineers
New York, New York, November 17-22, 1974

EXPERIMENTAL AND ANALYTICAL SONIC NOZZLE DISCHARGE COEFFICIENTS FOR REYNOLDS NUMBERS UP TO 8×10^6

ANDREW J. SZANISZLO

LEWIS RESEARCH CENTER, NATIONAL AERONAUTICS AND SPACE ADMINISTRATION
CLEVELAND, OHIO · 44135

ABSTRACT

Sonic discharge coefficients are presented for two different geometry flow nozzles using nitrogen gas at high pressures (100 atm ($100 \times 10^5 N/m^2$)) where real-gas correctons are significant. Throat Reynolds number range extended up to 8×10^6. Experimentally obtained coefficients for a nozzle with a continuous and finite radius of curvature agreed with those obtained analytically to within 0.2 percent. Experimental coefficients for a long-radius ASME nozzle agreed to within 1/4 percent to an empirical equation representing the most probable subsonic discharge coefficient.

INTRODUCTION

The sonic flow nozzle is now being recognized as an accurate, precise, and easy to use head-type of flowmeter for controlling and measuring the mass flow rate of gases over a wide range of flow. References [1 - 5][1] have pointed out the attractive and distinguishing features that make the sonic flow nozzle practical. Mass flow rate is easy to measure and control since it is directly proportional to upstream pressure level. Upstream pressure tap error is negligible since the approach velocity is usually small. Absence of a differential pressure measurement eliminates the throat tap and simplifies construction. Accuracy and ease of use are superior to a subsonic nozzle because the hard to make measurement of the small differential pressure at high

[1] Numbers in brackets designate references at end of paper.

pressures is not needed. Downstream pressure pulsations do not affect the mass flow rate because of sonic flow at the throat.

The above advantages of a sonic nozzle are now being utilized [6 - 11]. However, none of the above references have reported experimental C_D data at high-pressure levels where real-gas effects are significant (3 percent) and where the Reynolds numbers are as great as 1×10^7. Such data would demonstrate the accuracy of the technique of combining the analytical C_D values with the critical flow factors given by Johnson [12 - 15].

The experiment described below involve two different geometry flow nozzles operated over a Reynolds number range of 5×10^5 to 8×10^6. These high pressure (100 atm ($100 \times 10^5 N/m^2$)) experiments add new data to the scant amount reported in the literature on sonic flow nozzles and expands the range of sonic C_D values into the regime where real-gas corrections are significant. An additional objective was to analytically calculate the C_D for one of the above nozzles and compare the results to the experimental data.

APPARATUS AND TEST PROCEDURE

Sonic-Nozzle Geometries Selected

The first flow-nozzle geometry selected (fig. 1) had the traditionally recommended quadrant of an ellipse for the convergent section [16]. This section was tangent to a straight throat section of length 0.6 times the throat diameter. Nozzle inlet-to-throat area ratio was 5.5. The second flow-nozzle geometry represents a class of wall profiles having a finite and continuous radius of curvature from the inlet through the throat plane. In particular, circular-arc profiles which have a constant radius of curvature and are a subset of this class have been examined in references [3, 7, and 17]. Such profiles produce a continuous acceleration of the fluid along the wall which makes the analytical calculation of the sonic C_D tractable and less inaccurate. The design radius of curvature of the nozzle shown by figure 2 was 4 times the throat radius (normalized radius of curvature, $R_N = 4$). However, due to machining inaccuracies the radius of curvature of the nozzle utilized (fig. 2) was found to continuously increase in value from the throat plane to the inlet. The throat plane R_N for this nozzle had a value of 2.3 . Nozzle inlet-to-throat area was 7. Nozzle throat

diameter for both of the above nozzles was a nominal 0.25 inches (6.35×10^{-3} m). Throat diameter to upstream pipe diameter ratio, β, equaled 0.15 for both nozzles. And both nozzles were fabricated from free-machining stainless steel with a specified maximum surface roughness of 3.2×10^{-5} inches (8×10^{-7} m).

Nitrogen-Gas Flow Facility

A schematic drawing of the test facility is shown in figure 3. Nitrogen gas supplied from a portable trailer was throttled from 160 atm (160×10^5 newtons per square meter (N/m^2)) to the desired operating pressure levels which were varied from 5 atm ($5 \times 10^5 N/m^2$) to 100 atm ($100 \times 10^5 N/m^2$). Maximum flow rate was 1.7 lbm/sec (0.75 kg/sec). A bundle of tubes with each tube having a length-diameter ratio of 10 was used just downstream of the pressure regulator to minimize any swirl in the flow. A sharp-edged orifice (modification of ref. 18) was used as the working standard with a maximum differential pressure of 7 psi ($0.48 \times 10^5 N/m^2$). The orifice, 60-diameter-length approach pipe, and the 25 diameter-length downstream pipe were calibrated as an integral assembly on both water and air. Inaccuracy of the water stand used for this calibration was less than ± 0.2 percent.

Differential pressure across the orifice was determined with a fused-quartz Bourdon-tube precision pressure gauge [19]. Inaccuracy of this gauge is less than $\pm .05$ percent of full scale. The null output from the electro-optical transducer of the gauge was displayed on an oscilloscope and time averaged. Differential pressure lines were matched for time delay and appropriate volumes and sintered porous-metal snubbers were introduced in each line to equalize time constants. This filter network reduced differential-pressure measurement errors due to absolute pressure-level fluctations which had a root-mean-square magnitude of approximately 9 percent of the differential pressure before filtering. The final orifice differential pressure inaccuracy was determined to be less than ± 0.1 percent. At absolute-pressure levels greater than 30 atm ($30 \times 10^5 N/m^2$), the electro-optical transducer output of the gauge was corrected by a method described in reference [20].

The pipe section between the orifice and the nozzle test section as well as the nozzle test section itself were thermally insulated to give a uniform gas-temperature distribution across the nozzle inlet

plane. Orifice gas temperature was measured with a thermocouple probe 5.5 pipe diameters downstream of the orifice [21]. Nozzle inlet gas temperature was measured with a thermocouple probe 3.4 pipe diameters upstream of the nozzle inlet. Also, near this location the nozzle upstream static pressure was measured. Nozzle downstream pressure was measured about 1 pipe diameter downstream of the nozzle exit plane.

The thermocouple electromotive force from the orifice and nozzle thermocouples were measured to a corresponding temperature inaccuracy of $\pm 0.4^{\circ}F$ ($\pm 0.2K$). Operating absolute-pressure levels inaccuracies of less than ± 0.1 percent were achieved by using four different sets of gauges, of the Bourdon type, to span the pressure range used and by having the gauges periodically recalibrated.

After instrument calibration and a slow pressurization of the facility to the maximum pressure level for the test to be run, system leak checks and instrument calibrations were performed. Nitrogen gas flow was then initiated by fully opening the throttle valve. The measured upstream to downstream pressure ratio across the test nozzle was always greater than 2 which insured that the flow through the nozzle was indeed sonic. Not until the temperature of the facility had stabilized, approximately 5 minutes later, were data taken. Each data point consisted of a 1 minute run at constant flow rate. The flow rate was then changed by reducing the nozzle upstream pressure with the pressure regulator.

ACCURACY AND REPEATABILITY

Accuracy

The overall relative inaccuracy associated with the value of C_D is found by combining the relative uncertainties previously stated for each variable. Variables considered are the orifice flow coefficient, orifice and nozzle areas (and the effect of thermal contraction on throat area), pressure levels, temperature levels, and the orifice differential pressure. Combining the relative uncertainties of the above mentioned variables for a throat Reynolds number of 1×10^6 (upstream pressure equals 11 atm ($11 \times 10^5 N/m^2$)) yields an overall root-sum-square error of $\pm .25$ percent [22].

Real-gas factor - This factor [12] corrects the conventional one-dimensional, isentropic flow relation used for calculating the main-stream mass flow rate by accounting for the variation of the ratio of

specific heat and the compressibility factor. Neglecting to use this critical flow-factor can give an error in mass flow rate exceeding 3 percent at a pressure level of 100 atm ($100 \times 10^5 N/m^2$) for nitrogen gas [23].

An approximate value for the uncertainty in the critical-flow factor is obtained by comparing two different sources for nitrogen gas [12, 15]. The comparison shows at a temperature of $35^{\circ}F$ (275K) and a pressure of 10 atm ($10 \times 10^5 N/m^2$) the critical-flow factor from reference 12 exceeds the value from reference 15 by .03 percent. Whereas at 100 atm ($100 \times 10^5 N/m^2$), the difference is 0.4 percent. This difference increases monotonically with pressure level. Accounting for this critical-flow factor uncertainty at a throat Reynolds number of 8×10^6 (upstream pressure equals 95 atm ($95 \times 10^5 N/m^2$)) increases the overall root-sum-square relative error to $\pm$0.44 percent. The critical-flow factors from reference 12 are used in this report.

Repeatability

A calibration consists of a set of data points ranging from the maximum to the minimum pressure level of any one of the four pressure-level ranges examined. Figure 4 represents the total number of data points from 20 individual calibrations for the long-radius flow nozzle and figure 5 with 21 individual calibrations for the continuous wall curvature nozzle. At a Reynolds number greater than 1.6×10^6, the repeatability is $\pm$0.2 percent for a 95-percent confidence band for a single calibration [24]. The confidence band for a single calibration is the band within which it is predicted that all the data points of the next calibration will lie with a 95-percent probability. Stated band widths for a single calibration and for the mean are determined from t-distribution statistical calculations using the finite number of data points existing at selected Reynolds numbers.

SONIC NOZZLE PERFORMANCE

Experimental Results

Accurate interpretation of sonic nozzle performance as revealed by the C_D curve shape and its level requires knowledge of the upstream velocity profile. As shown by Ferron [25], the more uniform the upstream velocity profile the lower the C_D value. Inlet flow to both of the

nozzles tested is regarded as fully-developed turbulent flow due to the nozzle upstream-pipe length-to-diameter ratio of 60. Also, the measured inlet-temperature profile variation is less than $2^{\circ}F$ (1K) at the lowest mass flow rate. This essentially uniform temperature profile is due to the thermal insulation placed on the upstream pipe wall.

Initial air calibration - Sonic flow nozzle C_D variation with throat Reynolds number at flow conditions where real-gas effects are small was determined for air by using the Lewis flow standards facility. The results are shown in figures 4 and 5. The Reynolds number is based on the viscosity of the gas upstream of the nozzle and nozzle throat diameter. As seen from figure 4, at the low Reynolds numbers, the level of the C_D curve agrees with the independent calibration obtained from the Lewis flow standards facility. This indicates systematic errors from instrumentation are negligible.

Long-radius ASME flow nozzle - A sufficiently high number of data points have been obtained that permits reliable calculation of the sonic nozzle C_D mean curve shape and the 95-percent confidence band for a single calibration and for the mean curve. The mean curve for the sonic C_D variation with Reynolds number for this nozzle is shown by figure 4. It ranges in value from .988 at a Reynolds number of 3×10^5 to .992 at a Reynolds number of 8×10^6. Several features are indicated by the variation in the mean C_D curve. First, starting at the low Reynolds number, the C_D value increases up to a Reynolds number of 1×10^6 which is most probably due to a decreasing boundary-layer thickness. Immediately following is a region of apparent transition from a laminar to a turbulent boundary layer. This region extends over a Reynolds number range of 8×10^5 to 2×10^6. As can be seen from the increased size (± 0.3 percent) of the 95-percent confidence band for a single calibration, the C_D value is relatively ill defined over this Reynolds number range.

The apparent transition is most likely promoted by the local adverse pressure gradient generated by the discontinuous wall-radius of curvature at the juncture of the convergent section with the cylindrical throat section [26]. After this region of apparent transition, the C_D curve monotonically increases in value with Reynolds number. At these Reynolds numbers the 95-percent confidence band for a single calibration is less than ± 0.15 percent. Also, the 95-percent confidence band for

the mean curve is ±0.05 percent.

A comparison of the sonic nozzle C_D mean curve to the best empirical curve fit equation [27] for subsonic C_D values is also shown by figure 4. From this comparison, the extent of valid representation, if any, for the sonic C_D mean curve by this empirical equation is obtained. The empirical equation yields the most probable subsonic C_D values for the long-radius ASME flow nozzle. This equation is limited to a maximum throat Reynolds number of 6×10^6 at which the C_D equals 0.993. Even though there exists a lack of similarity between the subsonic C_D curve shape and the sonic C_D mean curve shape, the most probable subsonic C_D values do represent the C_D values to an inaccuracy of 1/4 percent for the experiments reported herein.

Continuous curvature nozzle - the mean curve for the sonic C_D variation with throat Reynolds number is shown by figure 5. It ranges in value from 0.989 at a Reynolds number of 6×10^5 to 0.991 at a Reynolds number of 8×10^6. A feature shown by the shape of the mean curve is the apparent transition for the Reynolds number region below 1×10^6. Nevertheless, the exact shape of the mean C_D curve is uncertain at these low Reynolds numbers where there are few data points. This uncertainty is indicated by the value of the 95-percent confidence band for the mean curve increasing from ±0.04 percent at a Reynolds number of 1×10^6 to ±0.4 percent at a Reynolds number of 6×10^5. For Reynolds numbers greater than 1×10^6, the mean C_D curve monotonically increases in value at a greater rate than the long-radius flow nozzle mean curve. Consequently, from the above mentioned factors for this sonic nozzle geometry, the flow range examined which is free of ill-defined transition regions is noticeably greater than the flow range for the long-radius flow nozzle. At these higher Reynolds numbers, the 95-percent confidence band for a single calibration is less than ±0.2 percent.

Comparison to Analytical Results

Nozzle flow model - Only sonic nozzles with continuous and finite radius of curvatures are considered herein. The gas flow through the nozzle is divided into two different flow regions. One is the mainstream

gas-flow region that is treated as an irrotational, isentropic flow of a perfect gas. In this region, fluid acceleration near the wall and the resulting inertial forces produce a non-uniform velocity profile (sonic line curvature) at the throat. Vincent [17] shows that inertial effects can affect the C_D by as much as 1 percent. The second is the viscous flow region along the wall occupied by the boundary layer. The boundary layer can lower the C_D value by as much as 5 percent at low Reynolds numbers. The effect of each of these two regions on the value of the sonic C_D is separately analyzed.

The mainstream gas flow parameters across the nozzle throat plane are calculated by using a computer program based upon reference 28 for axisymmetric flow. Calculation results are dependent upon the following input variables: (1) normalized wall radius of curvature at the throat (R_N); (2) nozzle throat radius; (3) nozzle axial length; (4) specific-heat ratio of the gas; (5) boundary-layer displacement thickness at the throat. The normalized throat radius of curvature of the nozzle studied herein is equal to 2.3 . Actual wall profile, which is not a circular arc, is piecewise curve fitted by the program from reference [29] which enables the wall Mach number distribution to be determined.

Two-dimensional, boundary-layer parameter values are determined by a computer program from reference [30]. The above mentioned wall Mach number distribution serves as part of the input data to this boundary-layer program. Laminar calculations are based upon the work of Cohen and Roshotko [31]. And the work of Sasman-Cresci [32] is used as the basis for the turbulent boundary-layer calculations. Modifications to this program with real-gas subprograms of reference [33] permit the accurate calculation of the speed of sound, gas density, and specific heat of nitrogen gas. Furthermore, transport property variation with pressure level is also accounted for by use of data from references [34-36]. The resulting boundary-layer displacemnt thickness at the throat is then used as part of the input to the above isentropic gas-core flow program for calculating the final value of the sonic C_D.

Analytical results comparison - The analytical sonic C_D variation with throat Reynolds number for the continuous curvature nozzle is shown

by figure 6 for nitrogen gas for both laminar and turbulent boundary-layer conditions. Also shown is the mean sonic C_D curve for the real-gas nitrogen flow data. Agreement between the analytical and experimental curves over the entire Reynolds number range experimentally investigated is good considering the previously discussed uncertainty in the mean C_D curve at the low Reynolds numbers. However, the analytical C_D variation for the laminar boundary layer differs from the Lewis in-house flow facility calibration by as much as 0.6 percent at the low Reynolds numbers. The difference between the analytical curve for the turbulent boundary layer and the mean C_D curve is equal to or less than 0.2 percent. This difference is within the mean C_D curve 95-percent confidence band for a single calibration. A comparison of the level and the slope of the analytical curves to the mean C_D curve tends to verify that the boundary layer is turbulent over the greater extent of the Reynolds number range covered. As previously stated, the experimental C_D value is determined by using a real-gas critical flow factor. Considering the previously discussed sources of error, it is seen that the sonic C_D for the nozzle tested can be determined to practical flow metering accuracy by the results from the turbulent boundary-layer calculations including real-gas effects. Therefore, the sonic C_D for any nozzle with a continuous and finite radius of curvature ($R_N > 2$) from the inlet to the throat plane can be expected to be represented over its practical Reynolds number range by the above analytical method for calculating the turbulent boundary layer. This assumes a corner exists at the inlet to augment early transition and thereby extend the useful Reynolds number range. Also, the installation of the sonic nozzle should be according to recognized standards. The ability to accurately calculate the C_D is highly desirable because it provides the sonic flow nozzle with the potential for becoming a compressible flow standard.

REFERENCES

1. Arnberg, B. T., "Review of Critical Flowmeters for Gas Flow Measurements." Journal of Basic Engineering, Trans. ASME, Ser. D, Vol. 84, No. 4, Dec. 1962, pp. 447-460.

2. Arnberg, B. T., Britton, C. L., and Seidl, W. F., "Discharge Coefficient Correlations for Circular-Arc Venturi Flowmeters at Critical (Sonic) Flow." ASME Paper 73-WA/FM-8.

3. Stratford, B. S., "The Calculation of the Discharge Coefficient of Profiled Choked Nozzles and the Optimum Profile for Absolute Air Flow Measurements." Journal of the Royal Aeronautical Society, Vol. 68, No. 640, April 1964, pp. 237-245.

4. Kastner, L. J., Williams, T. J., and Sowden, R. A., "Critical-Flow Nozzle Meter and Its Application to the Measurement of Mass Flow Rate in Steady and Pulsating Streams of Gas," Journal Mechanical Engineering Science, Vol. 6, No. 1, 1964 pp. 88-98.

5. Peignelin, [illegible] G., "Calibration of High Pressure Gas Meters with Sonic Nozzles," Journal of the Institute of Measurement and Control," Vol. 5, No. 11, Nov. 1972, pp. 440-446.

6. Varner, C. R., "A Multiple Critical Flow Venturi Airflow Metering System for Gas Turbine Engines." ASME Paper 69-WA/FM-5.

7. Smith, R. E. Jr., and Matz, R. J., "A Theoretical Method of Determining Discharge Coefficients for Venturis Operating at Critical Flow Conditions." Journal of Basic Engineering, Trans. ASME, Ser. D, Vol. 84, No. 4, Dec. 1962, pp. 434-446.

8. Godt, P. W., "Experimental Correlation of Air, Nitrogen, Helium and Argon Flowrates Through Critical Flow Nozzles." Paper presented at ISA 1st Symposium on Flow - Its Measurement and Control in Science and Industry, Pittsburgh, Pa., May 10-14, 1971.

9. Castillon, M. P., "Calibration of Gas Meters with Sonic Nozzles." Paper presented at ISA 1st Symposium on Flow - Its Measurement and Control in Science and Industry, Pittsburgh, Pa. May 10-14, 1971.

10. Schroyer, H. R., "Sonic Nozzles for Gas Meter Calibration, Part 1." Pipeline and Gas Journal, Vol. 200, No. 11, Sept. 1973, pp. 31-32.

11. Schroyer, H. R., "Sonic Nozzles for Gas Meter Calibration, Part 2." Pipeline and Gas Journal, Vol. 200, No. 13, Nov. 1973, pp. 64, 66, 68, 84.

12. Johnson, R. C., "Real-Gas Effects in Critical-Flow-Through Nozzles and Tabulated Thermodynamic Properties." NASA TN D-2565. 1965.

13. Johnson, R. C., "Calculations of the Flow of Natural Gas Through Critical Flow Nozzles." Journal Basic Engineering, Trans. ASME, Vol. 92, No. 3, Sept. 1970, pp. 580-589.

14. Johnson, R. C., "Real-Gas Effects in the Flow of Methane and Natural Gas through Critical-Flow Nozzles." NASA TM X-52994. 1971.

15. Johnson, R. C., "Real-Gas Effects in Critical Flow Through Nozzles and Thermodynamic Properties of Nitrogen and Helium at Pressures to 300×10^5 Newtons per square Meter (Approx. 300 atm.)." NASA SP-3046, 1968.

16. Bean, H. S., ed., Fluid Meters - Their Theory and Application. 6th edition, ASME, New York, 1971.

17. Vincent, J., "Sur la Determination d'un profile optimal de tuyere sonique. (Determination of an Optimum Profile for a Sonic Nozzle.)," Comptes Rendus of the Academy of Sciences, Ser. A, Vol. 267, Oct. 1968, pp. 614-616.

18. "Standards for Discharge Measurement with Standardized Nozzles and Orifices. German Industrial Standard, 1952," NACA TM-952. 1940.

19. Damrel, J. B., "Quartz Bourdon Gauge," Instruments and Control Systems, Vol. 36, Feb. 1963, pp. 87-89.

20. Szaniszlo, A. J., "Pressure Effect on the Sensitivity of Quartz Bourdon Tube Gauges," Review of Scientific Instruments, Vol. 43, No. 5, May 1972, pp. 816-817.

21. "Flow Measurement by Means of Thin Plate Orifices, Flow Nozzles and Venturi Tubes," PTC 19.5.5, ASME, 1959.

22. Doebelin, E. O., Measurement Systems: Application and Design, McGraw-Hill Book Co., Inc., New York, 1966, pp. 58-64.

23. Johnson, R. C., "Calculations of Real-Gas Effects in Flow Through Critical-Flow Nozzles," Journal Basic Engineering, Trans. ASME, Vol. 86, No. 3, Sept. 1964, pp. 519-526.

24. Dixon, W. J., Massey, F. J., Jr., Introduction to Statistical Analysis, 2nd edition, McGraw-Hill Book Co., Inc., New York, 1957.

25. Ferron, A. G., "Velocity Profile Effects on the Discharge Coefficient of Pressure-Differential Meters," Journal Basic Engineering, Trans. ASME, Ser. D, Vol. 85, Sept. 1963, pp. 338-346.

26. Hall, G. W., "Application of Boundary Layer Theory to Explain Some Nozzle and Venturi Flow Peculiarities," Institution of Mechanical Engineer, Proc., Vol. 173, No. 36, 1959, pp. 837-870.

27. Benedict, R. P., Most Probable Discharge Coefficients for ASME Flow Nozzles," ASME Paper 65WA/FM-1.

28. Kliegel, J. R., and Quan, V., "Convergent-Divergent Nozzle-Flows." AIAA Journal, Vol. 6, No. 9, Sept. 1968, pp. 1728-1734.

29. Smith, P. J., "FITLOS: A Fortran Program for Fitting Low-Order Polynomial Splines by the Method of Least Squares." NASA TN D-6401, 1971.

30. McNally, W. D., "Fortran Program for Calculating Compressible Laminar and Turbulent Boundary Layers in Arbitrary Pressure Gradients." NASA TN D-5681, 1970.

31. Cohen, C. B., and Reshotko, E., "The Compressible Laminar Boundary Layer with Heat Transfer and Arbitrary Pressure Gradient." NACA TR-1294, 1956.

32. Sasman, P. K., and Cresci, R. J., "Compressible Turbulent Boundary Layer with Pressure Gradient and Heat Transfer." AIAA Journal, Vol. 4, No. 1, Jan. 1966, pp. 19-25.

33. Johnson, R. C., "Calculation of Supersonic Stream Parameters of a Real Gas from Measurable Quantities Using Fortran IV Routines." NASA TN D-7653, Apr. 1974.

34. Hilsenrath, J., et. al., Tables of Thermodynamic and Transport Properties of Air, Argon, Carbon Dioxide, Carbon Monoxide, Hydrogen, Nitrogen, Oxygen, and Steam, Pergamon Press, New York, 1960.

35. Lenoir, J. M., and Comings, E. W., "Thermal Conductivity of Gases-Measurement at High Pressure," Chemical Engineering Progress, Vol. 47, No., 5, May 1951, pp. 223-231.

36. Lenoir, J. M., Junk, W. A., and Comings, E. W., "Measurement and Correlation of Thermal Conductivities of Gases at High Pressure," Chemical Engineering Progress, Vol. 49, No. 10, Oct. 1953, pp. 539-542.

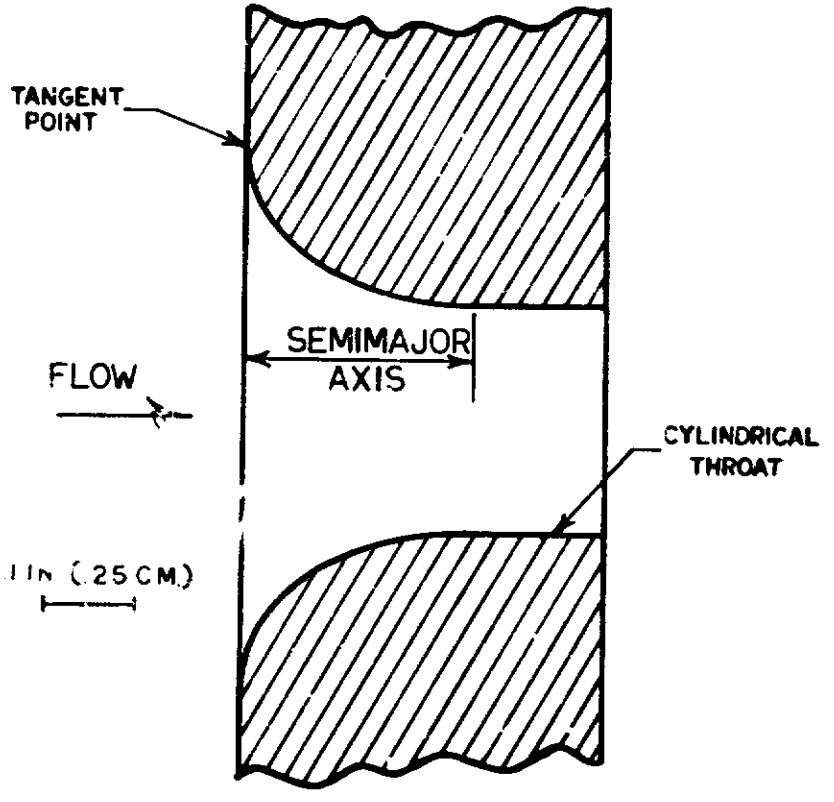

Figure 1. - Long-radius ASME sonic flow nozzle.

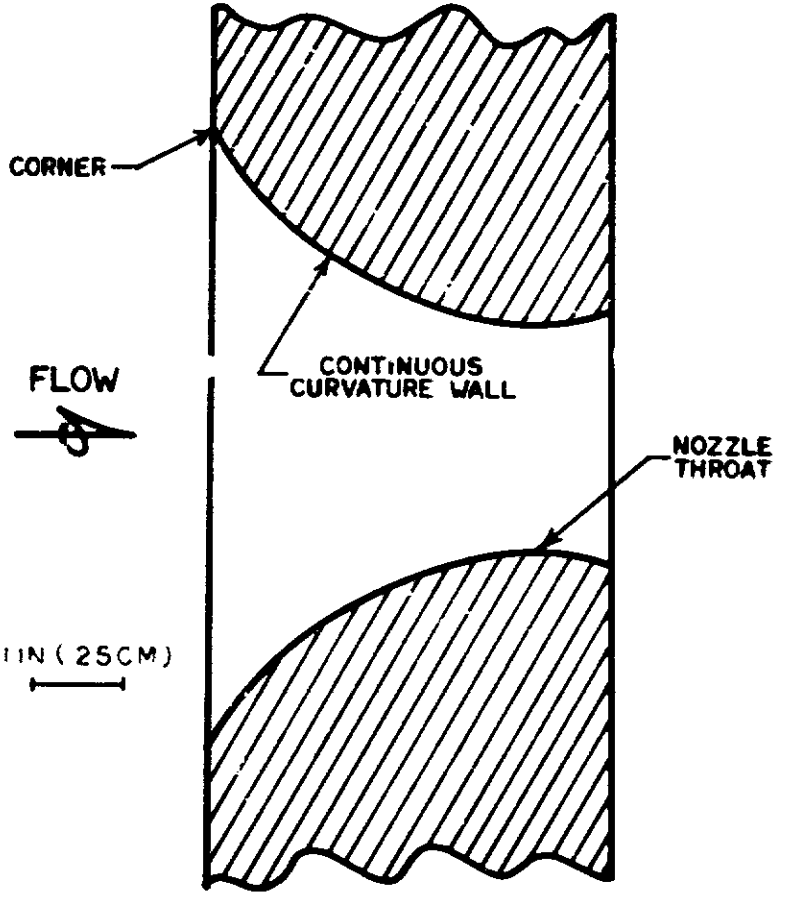

Figure 2. - Continuous wall-curvature sonic flow nozzle.

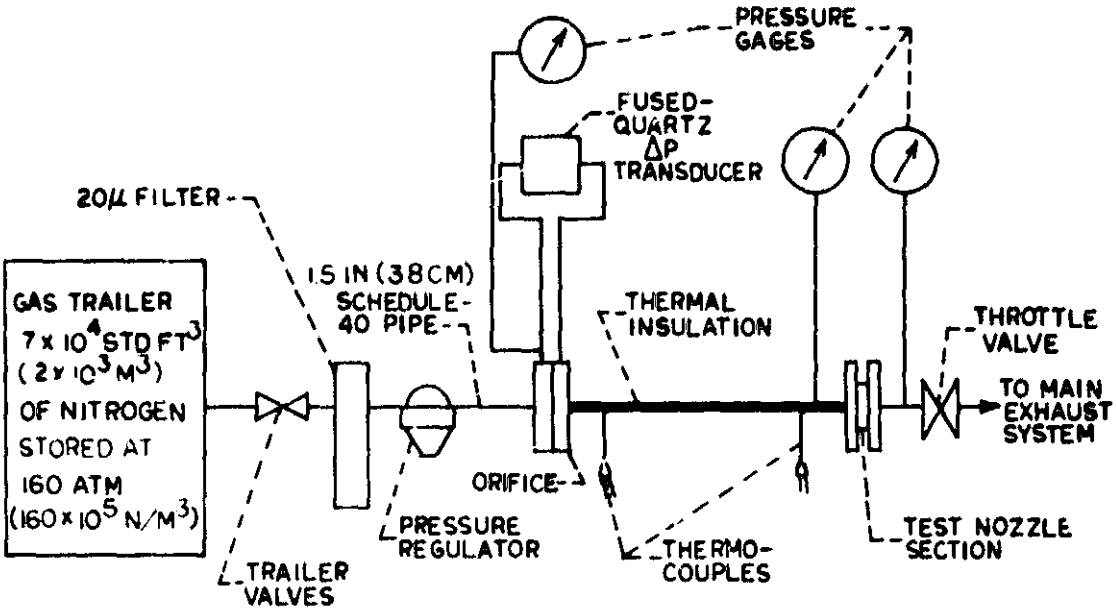

Figure 3. - Nitrogen-gas-flow facility for sonic flow nozzles.

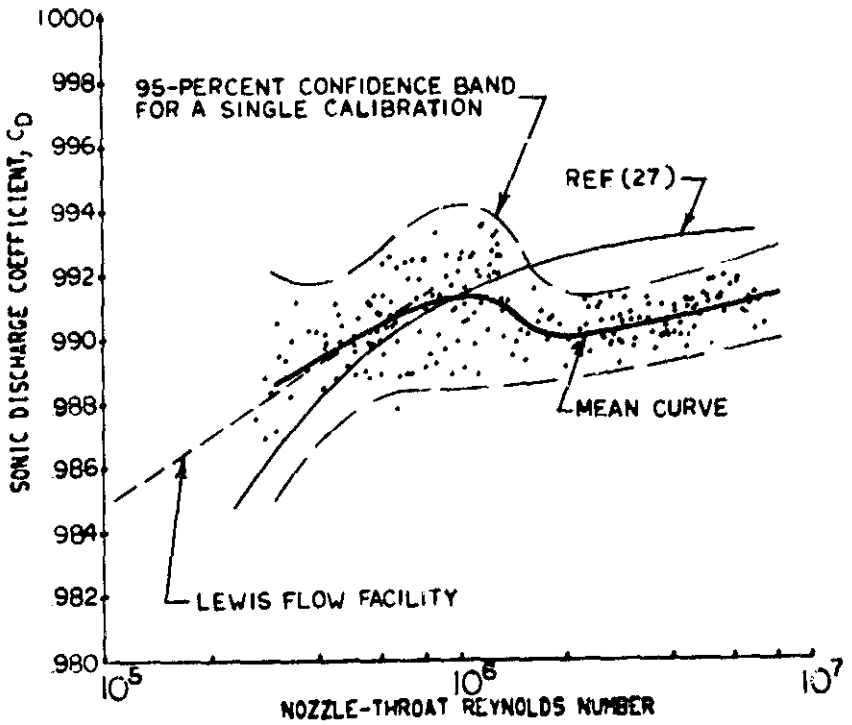

Figure 4. - Experimental discharge coefficients for the long-radius ASME flow nozzle using nitrogen gas.

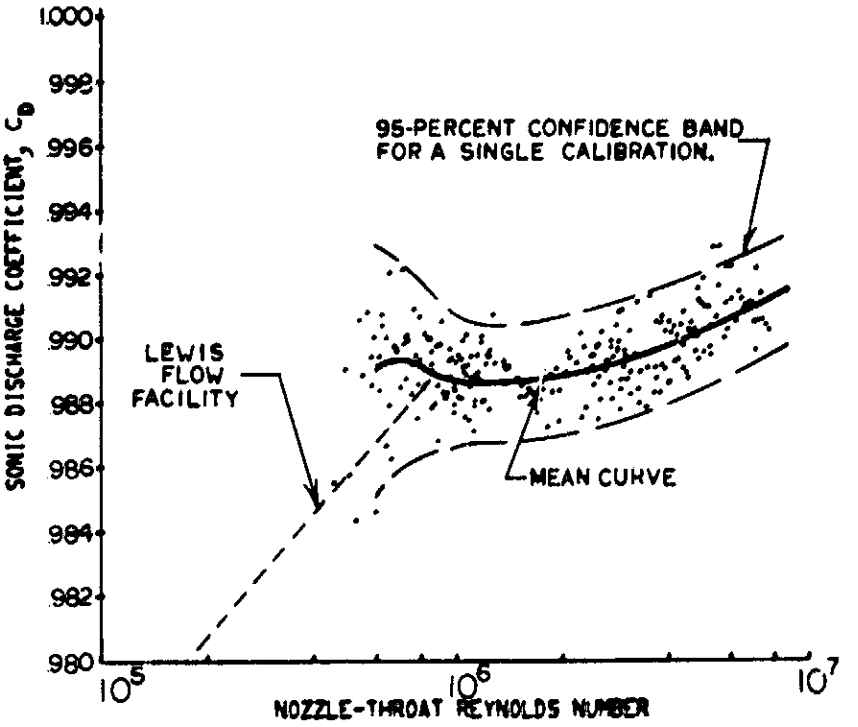

Figure 5. - Experimental discharge coefficients for the continuous wall-curvature sonic flow nozzle using nitrogen gas.

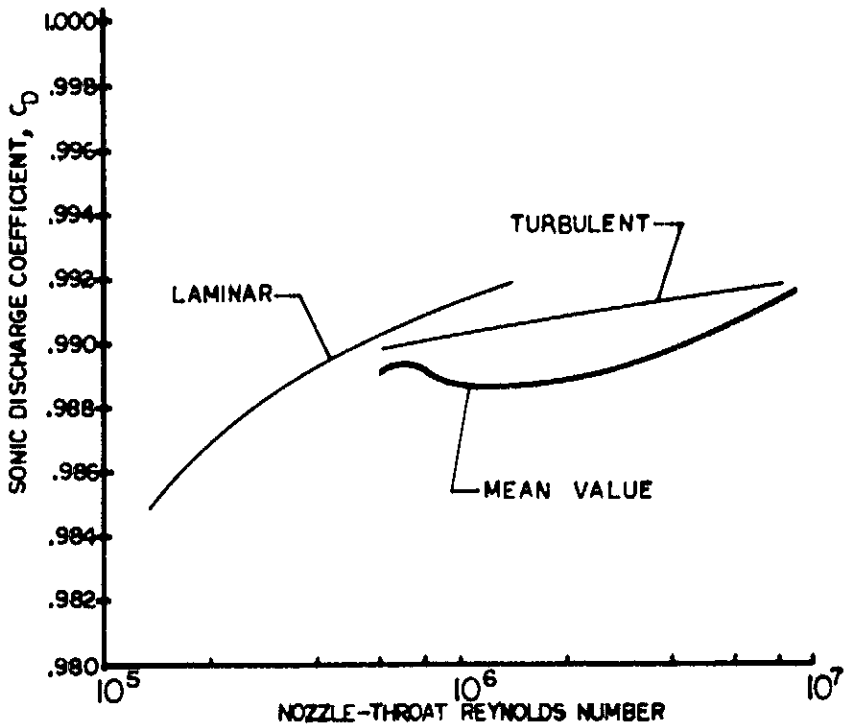

Figure 6. - Comparison of the analytical results to the experimental mean-value curve for the continuous wall-curvature sonic flow nozzle.

NASA-Lewis